ELSEVIER

Nuclear Instruments and Methods in Physics Research A 469 (2001) 95–105

NUCLEAR INSTRUMENTS & METHODS IN PHYSICS RESEARCH Section A

www.elsevier.com/locate/nima

The construction and operating characteristics of a cathode strip chamber system designed to measure the reaction vertices of a stopping kaon beam

M.W. Ahmed[a,*], D. Androic[b], I. Bertovic[b], J. Bjoraker[c], R. Chrien[d], X. Cui[a], D. Dehnhard[c], A. Empl[a], M. Furic[b], J. Gerald[c], R. Gill[d], E.V. Hungerford[a], H. Juengst[c], K.J. Lan[a], J.H. Liu[c], C.L. Morris[e], J.M. O'Donnell[c], J.C. Peng[e], T. Petkovic[b], P. Pile[d], M. Planinic[b], C.M. Riedel[e], A. Rusek[d], R. Sutter[d], L. Tang[f], H.A. Thiessen[e], M. Youn[a], V. Zeps[g]

[a] *Department of Physics, University of Houston, 4800 Calhoun, Houston, TX 77204-5506, USA*
[b] *Department of Physics, University of Zagreb, Bijenicka 32 HR, 10000 Zagreb, Croatia*
[c] *School of Physics & Astronomy, University of Minnesota, 116 Church St. SE, Minneapolis, MN 55455, USA*
[d] *Brookhaven National Laboratory, Department of Physics, Upton, NY 11973, USA*
[e] *Los Alamos National Laboratory, Los Alamos, NM 87545, USA*
[f] *Hampton University, 12000 Jefferson Avenue, Newport News, VA 23606, USA*
[g] *Department of Physics, University of Kentucky, Lexington, KY 40506, USA*

Received 28 November 2000

Abstract

The design, construction, and performance of a segmented-target, cathode-strip, tracking-detector is discussed. The chamber was made of low-Z materials in order to allow photons to leave the target region. It was used to determine the reaction vertex of stopping kaons, and was successfully operated in a high-intensity kaon beamline at the Alternating Gradient Synchrotron at Brookhaven National Laboratory. The vertical and horizontal resolutions of the stopping kaon reaction positions were $\sigma_X \sim 0.454$ mm and $\sigma_Y \sim 1.180$ mm, respectively. The uncertainty in the longitudinal (Z) direction is given by one-half the thickness of a target segment.

PACS: 29.40.Gx; 29.40.Cs; 21.80.+a

Keywords: Cathode-strip detector; Stopped kaons; Hypernucleus; NMS

1. Introduction

It is possible, within multiple scattering errors, to obtain the transverse position of each particle in a beam as it passes through a target by determining its incident trajectory. However, it is not

*Corresponding author. Tel.: 1-713-743-3502; fax: 1-713-743-3589.

E-mail address: mahmed@uh.edu (M.W. Ahmed).

0168-9002/01/$ - see front matter
PII: S0168-9002(01)00705-7

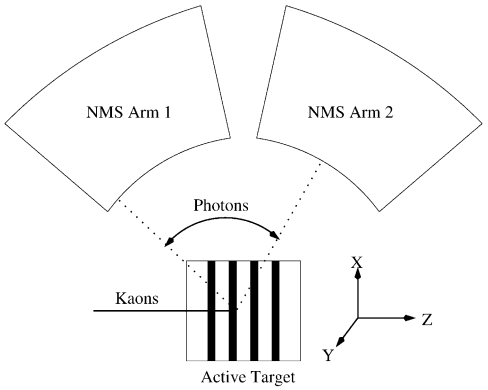

Fig. 1. A schematic diagram for the detection of a π^0 in experiment 907 at BNL.

always possible to know where, along a trajectory, a reaction has occurred. This paper reports on the construction and operational characteristics of a segmented-target, cathode-strip proportional counter designed to track a stopping kaon to its reaction vertex.

An active target chamber (ATC) was used to obtain the vertex of the reaction $(K^-_{stopped}, \pi^0)$ when a beam of kaons is brought to rest in a set of 12.7 mm thick, segmented, solid-carbon targets. In our experiment, the above reaction produces a recoiling hypernucleus and a π^0. The π^0 is detected by measuring the energy and position of each of the two decay photon showers in two out-of-beam crystal arrays of the Neutral Meson Spectrometer (NMS) [1]. Fig. 1 shows the setup of the apparatus at the C8 kaon beamline of the Alternating Gradient Synchrotron (AGS) at Brookhaven National Laboratory (BNL). Using the conversion points of the photons and the position of the reaction vertex, the opening angle of the two-photon decay and thus the energy of the π^0 was determined to higher accuracy than is possible by measurement of the energies deposited in the crystal arrays.

The resolution of the opening angle measurement dictates the energy resolution of the π^0 detection. The opening angle in turn depends on the ATC vertex and the NMS conversion point measurements. We focus here on the error in the opening angle measurement arising from the position error in the ATC stopping vertex. For a given location of the vertex in the ATC, the contributions of the errors in the three stopping coordinates to the error in the opening angle measurement are not the same. For the configuration shown in Fig. 1, the X-vertex position resolution contributes more than the Y and Z resolutions to the opening angle resolution. A Monte Carlo of the π^0 decay process showed that the desired missing mass resolution ($\leqslant 2$ MeV/c^2) requires that the σ_X needs to be less than 1 mm, σ_Y less than 2 mm, and $\sigma_Z \sim 6$ mm [2]. In order to achieve these position resolutions, longitudinal tracking becomes important due to low-energy kaon multiple scattering in the target and the angular spread of the beam. Therefore, an alternating set of segmented targets and wire chambers was employed to obtain both transverse and longitudinal position of the beam particles. It was this information that the ATC was designed to provide. The σ_X and σ_Y constrain the transverse resolution required from the ATC, and $\sigma_Z \sim$ 6 mm correspond to using the longitudinal tracking of the ATC to locate the interation point within a 12 mm thick target segment.

The NMS detects the two photons from the decay of the reaction π^0's and the ATC should minimize the probability that these photons convert or otherwise interact before reaching the detector arrays. Furthermore, the ATC geometry must maximize the number of kaons available to react in the target. Thus the design constraints on the ATC require that: (1) the ATC must determine the reaction vertex within the constraints given above; (2) the ATC must be constructed so that it presents little material to the decay photons in leaving the target region; (3) the ATC must catch a substantial fraction of the diverging kaon beam as it exits a degrader upstream of the ATC; and (4) the ATC must contain sufficient target material to provide a reasonable reaction yield.

2. Construction

To satisfy the design criteria described above, the ATC was composed of a number of laminated detector-target units capable of being assembled in several ways. For our purposes, we found it most

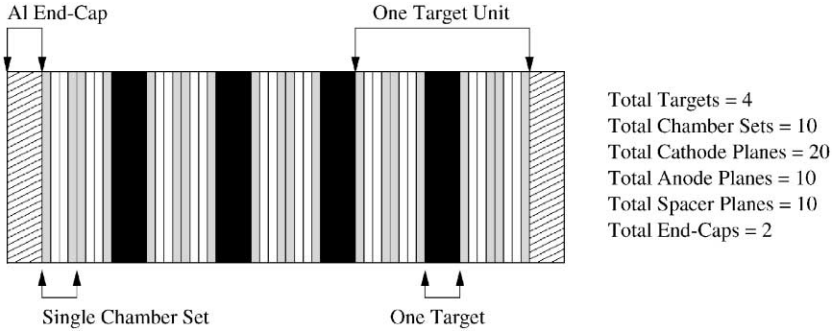

Fig. 2. A conceptual side view of the ATC.

useful to sandwich a thin stopping target between two sets of cathode-strip readout wire chambers (CSC), and repeat this geometry until the combined target thickness was sufficient to stop most of the kaon beam, Fig. 2. The targets[1] were planar and were placed within a polyethylene holder mounted in the ATC frames. Each CSC supplied two-dimensional position information on penetrating charged particles, allowing all charged-particle track vectors to be reconstructed. Table 1 summarizes the parameters of the ATC.

2.1. Mechanical construction of the ATC frames

To minimize the material thickness, the detector frames were constructed of 3.175 mm polyethylene sheets having a radiation length of ~ 480 mm. If a conventional material such as G-10 with a radiation length of ~ 190 mm had been used, the probability that at least one of the two photons interacted in the frames would have been $\sim 20\%$, as opposed to the $\sim 8\%$ for the polyethylene. However, to provide the electrical connections on each chamber plane, a thin, 0.254 mm, G-10 sheet with etched lands was attached to the polyethylene (see Fig. 3). Since the NMS photon detector was placed either above or below the ATC, the frame thickness in these dimensions was minimized, requiring all external electrical connections to the chamber to be made from the sides.

Table 1
ATC parameters

Total number of the targets	4
Thickness of individual targets	12.7 mm
Target material	Graphite
Total number of cathode planes	20
Thickness of single cathode plane	3.429 mm
Thickness of cathode foil	0.0127 mm
Number of cathode strips per plane	64
Capacitance between two strips	12 pF
Single strip resistance	0.11 Ω/mm
Total number of anode planes	10
Thickness of a single anode plane	3.429 mm
Anode wire diameter	0.02 mm
Wire material	gold-plated tungsten
Average anode wire tension	72 g
Anode potential	2.2 kV
Total number of spacer boards	10
Thickness of spacer boards	3.429 mm

After many attempts, it was found that double sided carpet-tape[2] of thickness ≈ 0.1 mm provided a reliable method to attach the G-10 sheet to the polyethylene frame. The use of this tape created a flexible bond which allowed reasonable handling and clamping of the non-rigid chamber frames. The polyethylene surface was sand-blasted before applying the tape to provide better adhesion. A thin bead of epoxy[3] was placed along the inner edge of the detector frame, between the G-10 sheet and the polyethylene, to prevent out-gassing

[1] Graphite Target, GRADE G11, Graphite Engineering & Sales Co., 712 Industrial Park Dr., Greenville, MI 48838, 1-800-472-3483.

[2] Scotch, 1.5 inch Carpet-Tape, 3M Do-It-Yourself Division.

[3] PolyStrate, 2-Ton Epoxy 14260, ITW Devcon, Denvers, MA 01923.

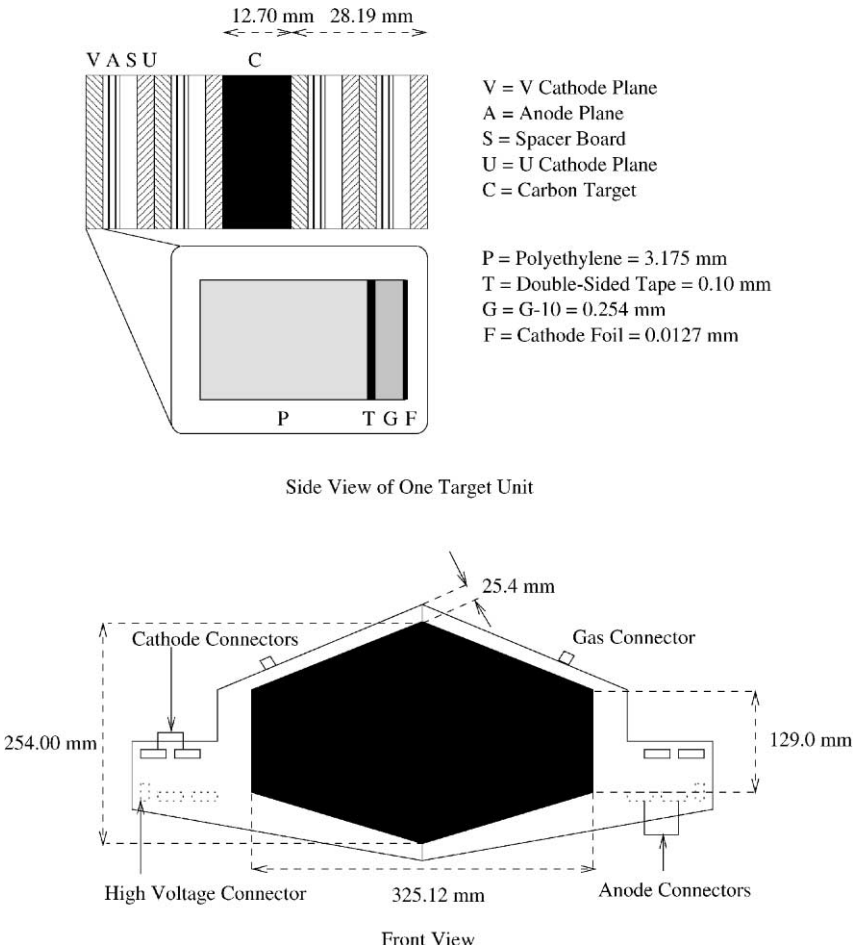

Fig. 3. A conceptual side and front view of the ATC.

and to protect the tape adhesive from reacting with the chamber gas.

In order to align all the ATC frames with respect to one another, holes were drilled through fiducial marks on G-10 sheets for both anode-wire and cathode-strip planes. Steel pins were placed through these holes and were rigidly fixed in aluminum end-plates placed on either side of the ATC array. The end-caps were machined from 12.7 mm Al tooling plate, and provided extremely flat, parallel surfaces which held the chamber frames planar when they were pressed together. Voids were machined in these plates to remove as much material as possible, without compromising the mechanical rigidity of ATC system.

Each frame was fitted with a 1 mm viton "O" ring to gas-seal the system when assembled. Gas entered and exited through fittings in the Al end-caps and was required to flow serially through each separate chamber of the detector. The detector not only was pinned together as described above, but was bolted tightly by long, 3.175 mm drill rods, which helped detector alignment, and pressed the frames flatly against the Al end-plates.

2.2. Cathode planes

As described in the previous section, a cathode plane was made by attaching a 3.175 mm polyethylene frame to a 0.254 mm G-10 sheet. The

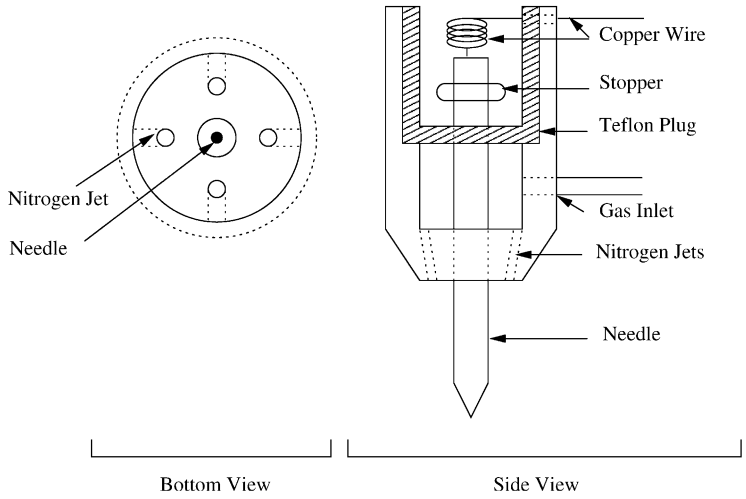

Fig. 4. Assembly for the EDM.

G-10 sheet provided the etched leads connecting the foil attachment points to a signal connector outside the detector frame. Cathode foils, 0.9 μm gold-coated 12.7 μm Kapton[4], were stretched and epoxied onto these frames using a vacuum foil stretcher. The readout strips on these foils were etched using an electric discharge method (EDM), which was studied in some detail.

The EDM current to etch the foils was provided by a current-limiting, adjustable DC power supply. The voltage was set to 10 V and a 20-Ω wire-wound power resistor was also used in series as a current-limiting device. The etching needle was a 2 g tungsten rod with a tip ground into a rounded point of radius ≈ 0.3 mm, and supported in a Teflon holder. Only the weight of the needle rested on the surface of the Au foil. The holder had gas holes so that jets of nitrogen gas converged at the position of the tip, Fig. 4. The entire apparatus was moved over the foil surface by a computer-controlled milling machine, CNC, at an optimum speed of 15 mm/s. Each cathode plane has 64 strips, 4.0 mm wide, and the readout was divided equally into 32 signals per chamber side. The strips were made at an angle of 68.34° with respect to the vertical anode wires, and the strips on opposing foils in a given CSC were mirror images, so that a 2-D readout was obtained, Fig. 5. Electrical connections between each strip and the G-10 lands were made with conducting epoxy[5]. Since the number of cathode strips in the entire detector system was 1280, a thin template was made with narrow slots which could be aligned with the strips and lands. The template was positioned with the help of alignment pins and conducting epoxy, which when wiped across the surface of the template, filled the slots making all connections simultaneously on one side of a cathode plane. The cathode foils were held at ground potential.

A description of the electrical characteristics of the CSC is described in the performance section below.

2.3. Anode planes

The anode planes were constructed in a way similar to the CSC as described above. The G-10 sheets for the anode planes were etched to provide external high-voltage (HV) connections to each individual anode wire. Supplying each wire sepa-

[4] G404960, 80–90 μm gold vacuum deposited on one side of 0.5 mil Kapton, SHELDAHL, INC, Northfeild, MN, 55057, (505)-663-8276.

[5] BiPax, TRA-DUCT, BA-2902 Conducting Epoxy, TRA-CON INC., Resin Systems Division, 45 Wiggins Ave., Bedford, MA, 01730.

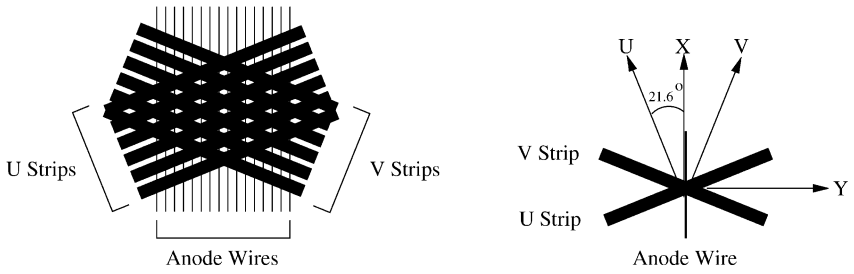

Front View of a CSC Section Coordinate System for the ATC

Fig. 5. Front view of a section of the ATC Cathode Strip Chamber. The ATC coordinate system in the plane perpendicular to the beam direction defined by the z-axis (into the page).

rately with a HV land allowed, in principle, the signal from the wires to be read at the same time as the foil strips. In addition, the wire voltage could be removed from a wire or section of wires, providing a way to keep part of the detector operational in the event of a broken wire. Each ATC anode frame had 128 gold-plated tungsten anode wires 0.02 mm in diameter. The wires were positioned vertically and spaced 2.54 mm apart. They were hand strung with an average tension of 72 g, and were first attached to the anode plane with epoxy, then connected to the G-10 lands by solder.

After the anode wires were strung, the tension was tested by measuring the mechanical resonance frequency of each wire [3]. This frequency is related to the wire tension by

$$T = 4\rho l^2 f_1^2. \quad (1)$$

In this equation, T is the tension, ρ is the mass per unit length, l is the length of the wire, and f_1 is the fundamental frequency. About 10% of the wires were found to have unacceptably low tension, and were replaced. An acceptable wire plane had an average wire tension of 65 ± 3 g, a drop of about 7 g below the wiring weight. When re-measured after a year of use at the AGS, the tension was found to average $\sim 55 \pm 3$ g, but this was still 5 times greater than that required to maintain the electro-mechanical equilibrium at the operational voltage of the chamber. Given measurement errors, this relaxation of the wire tension is not inconsistent with previous studies of the effect of creep in tungsten wires [4].

2.4. Spacer boards

All cathode planes were mechanically alike. The V plane is formed by rotating the U plane by 180° around the X-axis However, this rotation caused the spacing between the U to Anode plane and V to Anode plane to differ by the thickness of the cathode plane (polyethylene + G-10). Therefore, a polyethylene spacer frame of thickness 3.429 mm was inserted between an anode plane and a U plane to keep the anode–cathode distance for U and V cathodes the same. The spacer boards were also fitted with viton "O" rings on both sides to prevent gas leakage.

3. Electronics

The average capacitance between two adjacent strips was measured to be ~ 12 pF, while the resistance of an individual strip was measured to be $\sim 0.110\ \Omega$/mm. Cathode strips, in sets of 16, were connected by 1 m of 34-strand, flat ribbon-cable with alternating ground and signal wires, to a preamplifier card[6]. The trans-impedance preamplifiers then transmitted the analog signal from each strip through approximately 76 m of

[6] MP-10 16 CHANNEL AMPLIFIER, MP-10 Drawing Number 125Y-266500, Los Alamos National Laboratory.

twisted-pair cable, providing signal delay, to LeCroy FastBus ADCs. The signals were AC coupled into these ADCs by transformers to reduce low-frequency noise and ground loops. Although there were no DC offsets, AC coupling did create a long exponential tail of opposite polarity in the signal, extending well beyond the gate. This tail was small in amplitude and the cross-over was timed to occur approximately at the close of the gate (100 ns) for all channels. Pile-up was observed to be small, and the resolution did not change substantially with event rate. The overall charge gain of the electronics system was $\sim$ 55–60.

The relative gain of each channel must be known for the charge centroid determination. We obtained this calibration with a pulser, injecting a constant charge into the preamplifier between beam spills. This pulser automatically fed one of two charge levels to the inputs of a set of CSC channels comprising 1/8th of the system. Between each beam spill the pulse was sent to a different octal unit, and then recycled after all channels were pulsed. Limiting the calibration readout to 1/8th of the ATC at one time minimized the computer dead-time. This calibration resulted in two sets of lines in each ADC channel that allowed the slope and intercept to be determined. It was important to have two calibration points as the Fastbus readout used zero suppression, leaving the ADC channel-zero somewhat ambiguous. Variation in channel-to-channel gains was found to be $\approx$ 13% before application of the pulser calibration.

The cathode strips from the ATC were read out using 1280 electronics channels. In order to match the gains of these channels, a square voltage pulse ($\Delta V = 21$ mV, and $\Delta T = 200$ ns) induced a known charge, ΔQ, on each channel. Variation in channel-to-channel gains was found to be $\approx$ 13% before application of the pulser calibration. After the calibrations were applied, gain variations were reduced to approximately 3%, which were contributed from the electronic system noise.

4. Performance

The ATC was used at the low-energy separated beamline (LESB II-C8) of the BNL-AGS. The beam was tuned for a dispersed momentum focus at the position of a wedged degrader. The central momentum of the beam was $\sim$ 682 MeV/c and it had a relative momentum spread of $\Delta p/p$ of $\pm$5%. A wedge degrader of central thickness $\sim$ 141 mm was used to compensate the beam dispersion of $\sim$ 1.2 MeV/c/cm so that the momentum spread in the emerging kaons is minimized. The beam, optimized for kaons, also contained pions in a 3:1 (π/K) ratio for the positive and 19:1 for the negative beam polarities. The minimum ionizing pions penetrated the entire ATC with little multiple scattering. Passing pion and stopping kaon data of both charge polarities were taken to study the behavior of the ATC. The chamber operated with a humidified gas mixture of argon (60%) and iso-butane (40%), at a nominal anode potential of 2.2 kV. The average current drawn by 10 chambers was $\sim$ 28 μA from a typical 1.2 s beam spill of 6 million particles.

4.1. Pion data

Minimum ionizing pions were used to study the induced charge collection and distribution, operational efficiency, and position resolution of the ATC. The pions emerging from the degrader had a mean momentum of $\sim$ 500 MeV/c ($\beta \sim$ 0.95), and a beam size (FWHM) of $\sim$ 80 mm vertical, and 200 mm horizontal. The total charge deposited in the chamber gas by a minimum ionizing particle (MIP) was measured to be 16.8 pC, compared to the calculated value of $\sim$ 18 pC from a MIP producing 40 electrons, or 20 ion pairs and a gas gain of approximately 10^5. There have been a number of studies of the shape of the induced charge distribution in a CSC [5–8]. We used the semi-empirical equation of Ref. [7] to determine the expected width of the distribution, and thus determine the required strip width for our CSC design. This calculation indicated that we could expect significant charge collected on 3–5 strips. In our analysis of the data from the chambers we used the charge-weighted average method to determine the centroid of this charge distribution. While better algorithms are possible, this was the simplest, and for our purposes, provided sufficiently accurate positional

information. The induced charge distribution on cathode planes was found to be Gaussian with a FWHM of ~ 6 mm and in excellent agreement with the above prediction.

In order to estimate the wire chamber efficiency, pion tracks with singular hit multiplicity were selected to avoid the ambiguities of multiple tracks. Chamber efficiencies were obtained by defining a track from hits in two sets of U and V planes, one set positioned as far upstream as possible and the other as far downstream as possible. The efficiency was then determined for all planes in-between, assuming that a true cluster centroid must lie within 12 mm of the defined track. The track defining planes were permuted in order to obtain all the efficiencies. The average plane efficiency was found to be $\sim 96\%$. Similarly, position residuals were obtained by fitting a straight line track through the available hits in sets of U and V planes and calculating the distance between the centroid of the cluster distribution on a plane and the fitted track. The fitted position resolution, averaged for the U and V planes, were found to be $\sigma_U \sim 0.380$, and $\sigma_V \sim 0.336$ mm, respectively.

4.2. Kaon data

Stopping K^+ were tracked in the ATC to compare the induced charge profiles and position resolutions with pion data. Moreover, a Monte Carlo study was performed to obtain the kaon tracking efficiency and stopping position resolution. Typically, a stopping kaon track was found to deposit ~ 36 pC on a single anode wire, more than twice the charge of minimum ionizing pions. The induced charge distribution was found to be similar to the pion case, as expected. The position residuals, which are a measure of multiple scattering in the target and the number of planes included in the track fitting, were obtained for the kaon data. Fig. 6 shows the kaon data position residuals for low-energy kaons transversing the ATC. A Gaussian fit to these distributions, averaged for U and V planes, yield σ_U, and σ_V of ~ 0.6 mm. Since stopping kaons suffer larger scattering angles as they transverse through each one of the targets, the position resolution is expected to be not as good as for pions. The resolutions in U and V translate into $\sigma_X = 0.454$ mm and $\sigma_Y = 1.180$ mm by the following relation:

$$\begin{pmatrix} X \\ Y \end{pmatrix} = \frac{1}{2\sin\theta\cos\theta} \begin{pmatrix} \sin\theta & \sin\theta \\ \cos\theta & -\cos\theta \end{pmatrix} \begin{pmatrix} U \\ V \end{pmatrix} \quad (2)$$

assuming no contribution in error from $\theta(\sim 21^\circ)$

$$\sigma_X = \frac{\sqrt{\sigma_U^2 + \sigma_V^2}}{2\cos\theta},$$

$$\sigma_Y = \frac{\sqrt{\sigma_U^2 + \sigma_V^2}}{2\sin\theta}. \quad (3)$$

Positive kaons, stopped in the ATC, sometimes decay into $\pi^+\pi^0$ (BR = 21.16%). If the initial K^+ is at rest, the π^+ pions have a kinetic energy of about 108 MeV ($\beta = 0.82$) so the π^+ is minimum ionizing. However as the kaon comes to rest its

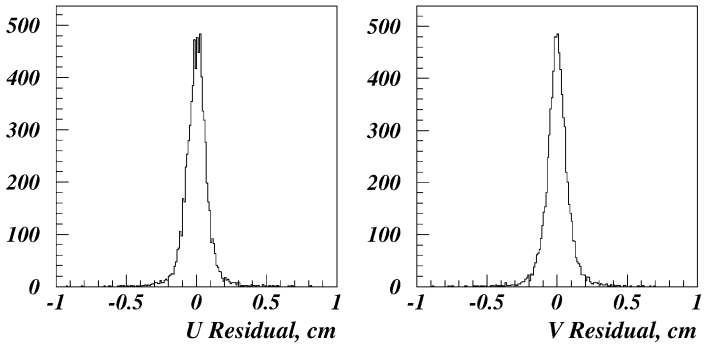

Fig. 6. Position residuals for the U and V cathode planes.

energy loss is significantly larger than the ionization caused by the π^+. Thus the appearance of a π^0 of energy $\approx$ 108 MeV in the NMS means that one should expect to find at most 2 charged particle tracks in the ATC coming from a common vertex. These tracks should have a sizable difference in the deposited energy in the wire chambers, although given the expected statistical fluctuations of the number of ion pairs per mm and the fact that most of the energy loss happens in the C targets, these differences may not be obvious.

The $\pi^0\pi^+$ decay of stopped K^+ provides a clean way to study the performance of the ATC. In order to locate the kaon stopping vertex, an incoming kaon track is constructed using the first two ATC chambers just before the first target. The track is then projected to the very last ATC chamber downstream of the last target. Hits along a cylinder of residual 8.0 mm in diameter from the projection are then identified. If no hits are found within this residual for both U and V planes in the two chambers after a target, then the kaon track is declared to have vanished and the target prior to the missing kaon track is chosen as the stopping target. All kaon hits leading up to the stopping target are fitted using linear regression and this fitted track is projected to the center of the stopping target.

A Monte Carlo study of the decay mode and the tracking algorithm was completed to obtain the tracking efficiency for the ATC. The Monte Carlo assumed all ATC planes to be 100% efficient in order to isolate the tracking efficiency from the operational efficiency of the ATC. Position residuals in X and Y directions between the target vertex, found by the tracking algorithm, and the actual decay position of the kaon were 0.330 and 0.833 mm, respectively. In addition, the efficiency of picking the correct stopping target was found by studying the Z position residual between the fitted track and the Z position of the kaon decay, Fig. 7. The probability of finding the correct stopping target Z was found to be $\sim$ 90%. Fig. 8 shows a single data event in which an incoming kaon was tracked to the stopping position. The outgoing π^+ is also tracked until it exits the ATC. An overall ATC vertex finding efficiency $\varepsilon_{\text{vertex}}$, which includes the plane efficiency ($\varepsilon_{\text{plane}}$) as well as tracking efficiency ($\varepsilon_{\text{tracking}}$), can be obtained if these efficiencies are statistically independent from

$$\varepsilon_{\text{vertex}} = \left[\sum_{i=r}^{p} \frac{p!}{i!(p-i)!}\varepsilon_{\text{plane}}^{p}(1-\varepsilon_{\text{plane}})^{p-r}\right]^{c} \varepsilon_{\text{tracking}} \tag{4}$$

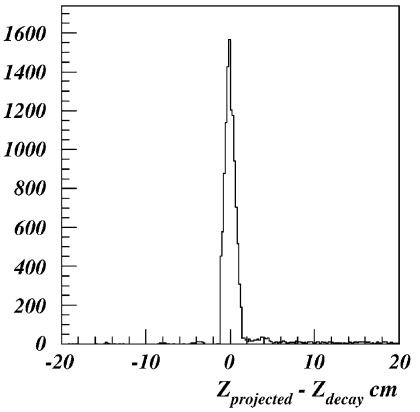

Fig. 7. Z Position residual between fitting algorithm and the actual kaon decay point. The width indicates the fact that Z cannot be measured to better than half target thickness.

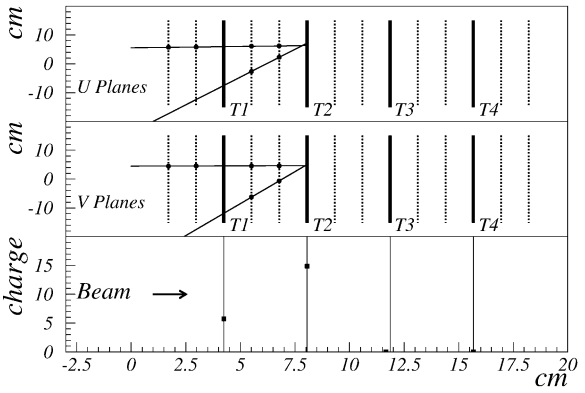

Fig. 8. A $K^+ \to \pi^+\pi^0$ event. Incoming K^+ (from the left) and outgoing π^+ (downward) tracks are seen in both U and V planes. A range curve is also shown with maximum charge deposition at the point of K^+ stop at the second target (T2).

where r is the minimum number of planes required out of a possible number of p in a coordinate to be able to track. In our case, we require at least 2 planes from a set of first 3 planes in a coordinate to successfully track. The number of independent coordinates required to track is $c = 2$ (1 U, and 1 V) for the ATC. The measured $\varepsilon_{\text{plane}} \sim 0.96$, and $\varepsilon_{\text{tracking}} \sim 0.90$ corresponds to an overall vertex finding efficiency of $\sim 88\%$.

The resolution of the π^0 energy measurement depends on the calorimetry of the NMS and the opening angle measurement between the two photons from the π^0 decay [9]. The opening angle measurement resolution in turn depends on the position measurement resolutions of the ATC and the NMS Wire Chambers [9]. A Monte Carlo study was performed to compare the expected and the measured energy resolution. ATC tracking resolutions of 0.330, 0.833, and 6.350 mm for σ_x, σ_x, and σ_z, respectively, were used as inputs for the Monte Carlo simulation. In addition, the simulation assumed γ conversion point resolutions in the NMS of 0.147, 0.120, and 3.175 mm for σ_x, σ_y, and σ_z, respectively. The calorimetry was scaled as a function of $\sqrt{E}$ to give a resolution of $\sigma_E = 6.5$ MeV at 245 MeV total energy. Fig. 9 shows the expected energy distribution from the predominant decay channel of the K^+ ($K^+ \to \pi^+\pi^0$) and the actual energy spectrum of the π^0 from the K^+ stops in the target. The energy resolution obtained from the Monte Carlo calculations is consistent with that of the experiment (Fig. 9).

The contribution of the ATC towards the total energy resolution depends on all three ATC coordinates, X, Y, and Z. However, due to the location of the ATC with respect to the NMS, the X coordinate resolution contributes the most towards the opening angle measurement of the photons and hence the pion energy. The need for the segmented active target is illustrated in Fig. 10. The solid curve shows the pion energy if the ATC was *not* segmented and hence had no longitudinal tracking. This curve is obtained by taking the transverse vertices from the measured entrance positions to the ATC and the longitudinal vertex at the center of the ATC. The energy resolution is degraded by a factor of ~ 3.8. The dashed curve shows the case if no information about the position of the stopping vertices was used and the target center was used to determine the opening angle of the π^0 decay. Fig. 10 should be

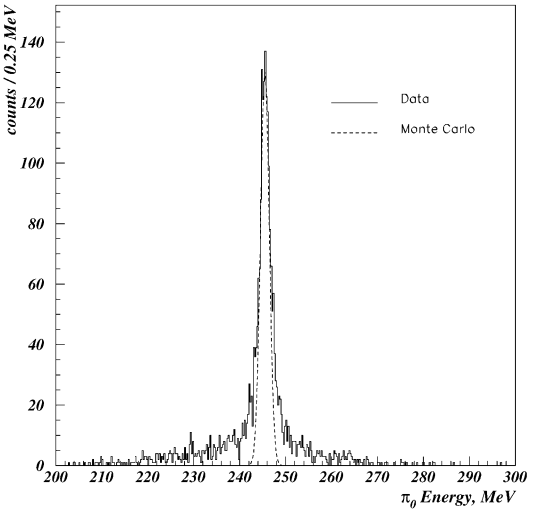

Fig. 9. A π^0 energy spectrum from the stopped K^+ is compared with the Monte Carlo of the predominant decay mode $K^+ \to \pi^+\pi^0$. The data and the Monte Carlo resolutions are consistent with one another. The FWHM is ~ 2 MeV.

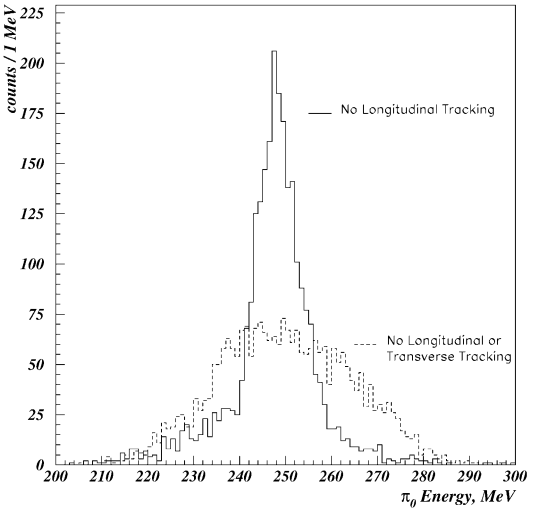

Fig. 10. A π^0 energy spectrum from the stopped K^+. The solid curve shows the case when longitudinal tracking of the ATC is not used in stopping vertex reconstruction. The dashed curve represents the case when both transverse and the longitudinal tracking is not used. This should be compared to Fig. 9 which shows the resolution when the stopping vertex is known for three coordinates.

compared to Fig. 9 when all information from the ATC is employed.

5. Summary

An Active Target Chamber (ATC) was successfully constructed, operated, and analyzed for AGS experiment 907. It was constructed using polyethylene as the frame-base material to reduce photon interactions in the ATC. The width of the induced charge distributions was found to be consistent with that predicted from a semi-empirical calculation. The position resolutions with a kaon beam, σ_u, σ_v, were found to be ~ 0.600 mm. Kaon tracking resolutions were estimated at $0.454, 1.180$ mm for σ_x, and σ_y, respectively, with σ_z of 6.35 mm. The reaction vertex was found with an efficiency of $\sim 88\%$. An energy resolution of $\leqslant 2$ MeV was achieved for π^0 detection using the K^+ stops. The performance of the ATC was found to be consistent with the expected results from Monte Carlo simulations.

Acknowledgements

We acknowledge the expert help of Hans Flick in the construction of the ATC. The late Yung-Chiang Lu, and Ed Meier provided valuable technical support during the ATC construction and testing. This work is supported in part by the US Department of Energy grants DE-AS05-76ER0-3948, DE-FG02-87ER40362, and DE-AC02-98CH-98CH10886.

References

[1] H.A. Thiessen, Jen-Chieh Peng, Investigation of light hypernuclei using the $(K^-_{stopped}, \pi^0)$ reaction, AGS PROPOSAL, E907, 1994.
[2] H. Baer, Computer program PIANG, Unpublished.
[3] N.J. Shenhav, Nucl. Instr. and Meth. A 324 (1993) 551.
[4] M. Barakat et al., Nucl. Instr. and Meth. A 349 (1994) 118; K. Fujita et al., Nucl. Instr. and Meth. A 308 (1991) 514.
[5] J.S. Gordan, E. Mathieson, Nucl. Instr. Meth. A 227 (1984) 267.
[6] J.R. Thompson et al., Nucl. Instr. and Meth. A 234 (1985) 505.
[7] E. Mathieson, Nucl. Instr. and Meth. A 270 (1988) 602.
[8] V. Radeka, R.A. Boie, Nucl. Instr. and Meth. A 178 (1980) 543.
[9] M.W. Ahmed, Doctoral Dissertation, 1999, University of Houston.